State Estimation and Vehicle Localization for the FIDO Rover

E. T. Baumgartner, H. Aghazarian, A. Trebi-Ollennu, T. L. Huntsberger, and M. S. Garrett

Science and Technology Development Section,
Jet Propulsion Laboratory,
California Institute of Technology, Pasadena, CA 91109

ABSTRACT

This paper describes the means for generating rover localization information for NASA/JPL's FIDO rover. This is accomplished using a sensor fusion framework which combines wheel odometry with sun sensor and inertial navigation sensors to provide an integrated state estimate for the vehicle's position and orientation relative to some fixed reference frame. This paper describes two separate state estimation approaches built around the extended Kalman filter formulation and the Covariance Intersection formulation. Experimental results from runs in JPL's MarsYard are presented in order to compare the state estimates generated using each formulation.

Keywords: rover localization, state estimation, extended Kalman filter, Covariance Intersection

1. INTRODUCTION

During future planetary exploration missions using robotic vehicles, knowledge of the rover's position and orientation relative to a fixed reference frame (typically, the reference frame attached to the system upon landing) is of great importance to the navigation of the rover relative to science targets located in the environment. Typical operations that rely on accurate knowledge of the rover's position and orientation include precision instrument placement onto rock and soil targets, rover navigation algorithms that include obstacle detection and avoidance, and instrument pointing for remote sensing. As such, planetary rovers carry a number of sensors that aid in the localization problem including wheel odometry, sun sensors, stereo vision sensors and inertial navigation sensors.

This paper describes the framework for determining estimates of the position and orientation associated with NASA/JPL's Field Integrated, Design and Operations (FIDO) rover. This rover is an advanced technology rover that is a terrestrial prototype of the rover that NASA/JPL plans to send to Mars in 2003. This vehicle carries an integrated instrument and sensor suite that mimics many of the instruments and sensors that the flight rover will carry. Additional details regarding the FIDO rover can be found in Baumgartner (2000)[1] and Schenker, et al (1998).[2] A picture of FIDO taken during a recent field trial held at Black Rock Summit in central Nevada is shown in Figure 1.

The primary framework for FIDO localization is based on the work presented in Baumgartner and Skaar (1994)[3] and Yoder, et al (1996),[4] that utilizes a time-independant extended Kalman filter formulation for the determination of the rover's state estimates. In addition to the extended Kalman filter formulation, this paper will also describe the implementation of a new approach to linear and non-linear estimation known as Covariance Intersection.[5] This sensor fusion approach is unique in its ability to produce consistant and conservative estimates in the presence of unmodelled correlations between the state and sensor measurements or between time-ordered sensor measurements. The primary sensors utilized in the current FIDO state estimation approach include wheel odometry and the sun sensor with the inertial navigation sensors providing attitude information regarding the rover's pitch and roll angles about a gravity vector. Additional techniques that involve registering successive stereo-based range maps to determine a rover's traverse distance including work by Olson (2000),[7] Hoffman, et al, (1999)[6] and Matthies (1987)[8] are not included in the state estimation approach described in this paper although the inclusion of the outputs from these visual techniques can be easily accomplished using the proposed estimation framework.

In Section 2, the state estimation framework is described including the propagation of the state estimates using wheel odometry and the update of the state estimates using either the extended Kalman filter approach or the

Send correspondence to E. T. Baumgartner, E-mail: Eric.T.Baumgartner@jpl.nasa.gov.

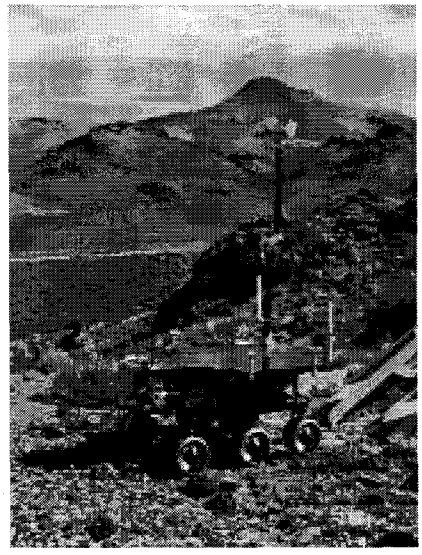

Figure 1. The FIDO rover at Black Rock Summit, Nevada in May 2000.

Covariance Intersection approach. Section 3 provides details concerning the particular sensors utilized on the FIDO rover for the localization problem. Experimental results are presented in Section 4 and the paper provides some concluding remarks in Section 5.

2. STATE ESTIMATION FRAMEWORK

This section describes the means for generating estimates of the rover's position and orientation based on both Extended Kalman Filter (EKF) formulation and the Covariance Intersection (CI) state estimation formulation. Underlying both of these techniques is the propagation of the state estimates based on wheel odometry. These propagated state estimates are then updated using acquired observation information through either the EKF or the CI update equations.

2.1. Propagation Equations

For the FIDO rover, the nominal vehicle motion consists of a straight drive or a turn-in-place about the center of the vehicle. The rover is capable of performing arc turns (both continuous and discrete motion) based on Ackerman steering, however, for flight applications, only a straight drive and a turn-in-place motion is allowed primarily due to power consumption concerns. Therefore, for this paper, the rover is restricted to this mobility mode. Also, for this paper, the rover state is defined as the planar position of the rover, (X,Y), and the orientation or heading angle relative to a north-aligned reference frame, (ϕ), as shown in Figure 2.

For a straight drive, the state equations that describe the motion of the rover based on wheel odometry alone is described by the following equations:

$$\frac{d\mathbf{x}(\alpha)}{d\alpha} = \begin{bmatrix} \frac{dX(\alpha)}{d\alpha} \\ \frac{dY(\alpha)}{d\alpha} \\ \frac{d\phi(\alpha)}{d\alpha} \end{bmatrix} = \begin{bmatrix} R\cos\phi(\alpha) \\ R\sin\phi(\alpha) \\ \frac{R}{B}u \end{bmatrix} + \mathbf{w}(\alpha) = \mathbf{f}(\mathbf{x}(\alpha), u) + \mathbf{w}(\alpha) \tag{1}$$

where $\mathbf{x} = [X\ Y\ \phi]^{\mathrm{T}}$, R is the nominal wheel radius, and B is half the distance between the wheel base. The independent variable, α, is defined as

$$\alpha = \frac{\theta_l + \theta_r}{2} \tag{2}$$

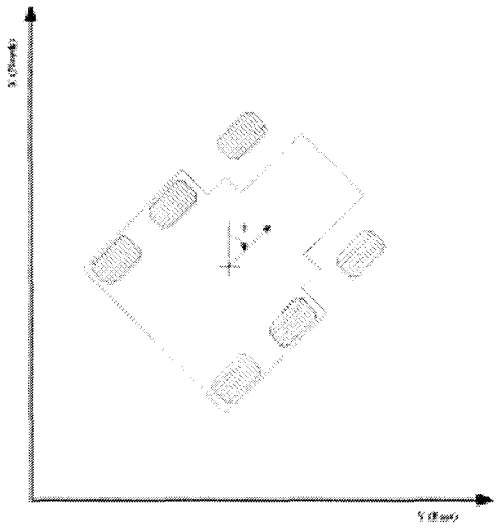

Figure 2. Rover coordinate frame.

where θ_l and θ_r are the average absolute wheel rotations of the left and right side wheels, respectively. The control variable, u is defined as

$$u = \frac{d\theta_l - d\theta_r}{d\theta_l + d\theta_r} \tag{3}$$

where $d\theta_l$ and $d\theta_r$ are the average differential wheel rotations of the left and right side wheels, respectively. The process noise, $\mathbf{w}(\alpha)$, is assumed to be a random process that captures the uncertainty in the state equations that is due to issues such as wheel slippage, etc.

The state equations given in Equation 1 are valid for all maneuvers except for a turn-in-place maneuver for which the independent variable, α, goes to zero and the state equations become singular. To handle this special case, α is re-defined as

$$\alpha = \frac{\theta_l - \theta_r}{2} \tag{4}$$

which results in the following state-equations for a turn-in-place maneuver:

$$\frac{d\mathbf{x}(\alpha)}{d\alpha} = \begin{bmatrix} \frac{dX(\alpha)}{d\alpha} \\ \frac{dY(\alpha)}{d\alpha} \\ \frac{d\phi(\alpha)}{d\alpha} \end{bmatrix} = \begin{bmatrix} 0 \\ 0 \\ \frac{R}{B} \end{bmatrix} + \mathbf{w}(\alpha) = \mathbf{f}(\mathbf{x}(\alpha)) + \mathbf{w}(\alpha) \ . \tag{5}$$

In either case, with the real-time sensing of the wheel rotations via wheel encoders, the above state equations can be numerically integrated (e.g. propagated) in real-time thereby producing the dead-reckoned estimates of the rover motion.

Likewise, the estimation error covariance matrix, $\mathbf{P}(\alpha)$, associated with the Kalman filter is propagated in real-time by the following

$$\frac{d\mathbf{P}(\alpha)}{d\alpha} = \mathbf{F}(\mathbf{x}(\alpha))\mathbf{P}(\alpha) + \mathbf{P}(\alpha)\mathbf{F}(\mathbf{x}(\alpha))^{\mathrm{T}} + \mathbf{Q} \tag{6}$$

where $\mathbf{F}(\mathbf{x}(\alpha))$ is the Jacobian of the state equations evaluated at the current value of the state and $\mathbf{Q}$ is the covariance matrix associated with the process noise. The process noise covariance matrix is assumed to be a diagonal matrix, i. e., $\mathbf{Q} = \mathrm{diag}[Q_{XX}, Q_{YY}, Q_{\phi\phi}]$, and, qualitatively, represents the confidence placed in the dead-reckoned estimates of the state.

2.2. Extended Kalman Filter Update Equations

The updated equations associated with the extended Kalman filter are given by

$$\hat{\mathbf{x}}(\alpha^+) = \hat{\mathbf{x}}(\alpha^-) + \mathbf{K}(\alpha^+)[\mathbf{z}(\alpha^+) - \mathbf{h}(\hat{\mathbf{x}}(\alpha^-)] \tag{7}$$

where the Kalman gain, $\mathbf{K}(\alpha^+)$, is

$$\mathbf{K}(\alpha^+) = \mathbf{P}(\alpha^-)\mathbf{H}(\hat{\mathbf{x}}(\alpha^-))^{\mathrm{T}}[\mathbf{H}(\hat{\mathbf{x}}(\alpha^-))\mathbf{P}(\alpha^-)\mathbf{H}(\hat{\mathbf{x}}(\alpha^-))^{\mathrm{T}} + \mathbf{R}]^{-1} \tag{8}$$

and where, in Equations 7 and 8, α^+ represents the value of α at which time a measurement is acquired and $\hat{\mathbf{x}}(\alpha^+)$ refers to the updated rover state. Also in these equations, $\hat{\mathbf{x}}(\alpha^-)$ represents the propagated state estimates produced by integrating forward the state equations given either by Equation 1 or by Equation 5 assuming zero process noise. In Equation 8, $\mathbf{H}(\hat{\mathbf{x}}(\alpha^-))$ is the Jacobian of the measurement equation which is evaluated at the propagated value of the rover state. Finally, the measurement noise covariance matrix is denoted by $\mathbf{R}$.

The estimation error covariance matrix is updated as follows

$$\mathbf{P}(\alpha^+) = [\mathbf{I} - \mathbf{K}(\alpha^+)\mathbf{H}(\hat{\mathbf{x}}(\alpha^-))]\mathbf{P}(\alpha^-) \tag{9}$$

where, in the above equation and in Equation 8, $\mathbf{P}(\alpha^-)$ represents the propagated estimation error covariance matrix produced by the integration of Equation 6.

2.3. Covariance Intersection Update Equations

As stated in the introduction, Covariance Intersection provides a new approach for data fusion that does not require any knowledge regarding the degree of correlation among the estimates and measurements.[5] Given a system mean and covariance estimate defined by $\{\mathbf{a}, \mathbf{P_{aa}}\}$ and the observation or measurement and its covariance estimate defined by $\{\mathbf{b}, \mathbf{P_{bb}}\}$, then the convex combination of the mean and covariance in the information (inverse covariance) space is defined by

$$\mathbf{P}_{cc}^{-1} = \omega\mathbf{P}_{aa}^{-1} + (1-\omega)\mathbf{P}_{bb}^{-1} \tag{10}$$

$$\mathbf{P}_{cc}^{-1}\mathbf{c} = \omega\mathbf{P}_{aa}^{-1}\mathbf{a} + (1-\omega)\mathbf{P}_{bb}^{-1}\mathbf{b} \tag{11}$$

where $\mathbf{c}$ is the updated mean and $\mathbf{P}_{cc}$ is the updated covariance estimate and where $\omega \in [0,1]$. The free parameter ω is determined by minimizing the determinate of $\mathbf{P}_{cc}$. According to the notation introduced in Section 2.2, $\mathbf{c} = \hat{\mathbf{x}}(\alpha^+)$, $\mathbf{P}_{cc} = \mathbf{P}(\alpha^+)$, $\mathbf{a} = \hat{\mathbf{x}}(\alpha^-)$, $\mathbf{P}_{aa} = \mathbf{P}(\alpha^-)$, $\mathbf{b} = \mathbf{z}(\alpha^+)$, and $\mathbf{P}_{bb} = \mathbf{R}$.

In terms of updating the state estimates using the acquired observations, the update equations for the CI algorithm are as follows

$$\hat{\mathbf{x}}(\alpha^+) = \hat{\mathbf{x}}(\alpha^-) + (1-\omega)\mathbf{P}(\alpha^-)\mathbf{H}^T\left((1-\omega)\mathbf{H}\mathbf{P}(\alpha^-)\mathbf{H}^T + \omega\mathbf{R}\right)^{-1}[\mathbf{z}(\alpha^+) - \mathbf{h}(\hat{\mathbf{x}}(\alpha^-)] \tag{12}$$

$$\mathbf{P}(\alpha^+) = \frac{1}{\omega}\left[\mathbf{P}(\alpha^-) - (1-\omega)\mathbf{P}(\alpha^-)\mathbf{H}^T\left((1-\omega)\mathbf{H}\mathbf{P}(\alpha^-)\mathbf{H}^T + \omega\mathbf{R}\right)^{-1}\mathbf{H}^T\mathbf{P}(\alpha^-)\right] \tag{13}$$

where it is assumed that in Equations 12 and 13 the matrix $\mathbf{H}$ is a function the propagated state estimates, i.e., $\mathbf{H} = \mathbf{H}(\hat{\mathbf{x}}(\alpha^-))$.

3. SENSOR SOURCES

On the FIDO rover, there are three primary sensor sources that are used to determine vehicle localization. These sensors are wheel odometry which is used to propagate the state estimates as in Section 2.1 and the sun sensor and inertial navigation sensors which are used to update the state estimates using either the EKF framework or the CI framework.

For wheel odometry, the FIDO drive system consists of independently driven actuators located in each of the 6 drive wheels on the vehicle. Each actuator is outfitted with a optical encoder that can resolve the rotation of a wheel to within 0.027 degrees which corresponds to a incremental wheel travel of 0.0485 mm for the 10 cm radius wheels on FIDO. All encoder data on the rover is collected at 200Hz and utilized at 50Hz as the feedback sensor for the closed-loop PID velocity and PID position control of all of the rover's actuators. At the 50Hz data rate, the propagation equations given in Equations 1 or 5 are integrated to produce the propagated state estimates assuming zero process

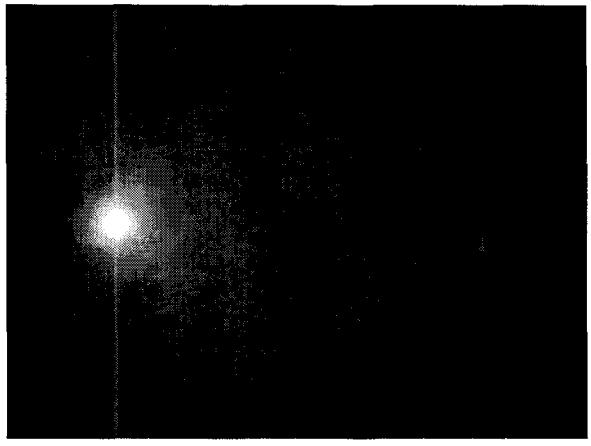

Figure 3. Representative sun sensor image.

noise. It should be noted that due to the wheel/ground interactions experienced by each of the rover's wheels as it traverses across a natural terrain setting, there is the possibility that wheels may "fight" one another as each wheel experiences a different loading/torque profile. To combat this phenomenon, a "velocity synching" approach has been implemented on the FIDO rover that seeks to maintain a nominal loading profile among all rover wheels by modifying both the velocity and travel distance of each wheel through a voting scheme that determines which wheels are deviating from the nominal rover traverse velocity. This approach provides the ability for coordinating the control of all rover drive wheels and has been very successful in minimizing the power required during driving.

The sun sensor on the FIDO rover consists of a CCD imager with a wide field-of-view lens (approximately 110 degrees) that is includes a neutral density filter in the optical path. A representative image from the sun sensor is shown in Figure 3. The centroid of the sun is determined using a thresholding and centroid finding algorithm with outlier rejection. Given the location of the sun in the 2D image plane of the CCD sensor, a ray vector from the sun sensor to the sun is determined through knowledge of the internal camera parameters. The sun sensor camera is modeled as a fish-eye camera/lens system[9] and the set of 21 camera parameters associated with this camera model are determined using a calibration procedure. With the ray vector to the sun determined with respect to the sun sensor frame, the ray vector is then transformed to a gravity-down rover reference frame using the attitude sensors that are part of the inertial navigation sensors described below. From the ray vector with respect to the rover frame along with knowledge of where the sun should appear in the sky given time of day and the position of the rover on the Earth's surface (latitude and longitude), the heading of the rover with respect to a north-aligned reference frame, ϕ, is determined.

In addition to the sun sensor, the inertial navigation sensor (INS) is integrated on the rover to provide attitude information (roll and pitch) along with attitude rate information (roll rate, pitch rate, and heading rate). This is accomplished using a commercial three axis accelerometer and gyroscope INS package. The rate sensors consist of vibrating ceramic plates that utilize the Coriolis force to output angular rate information that is independent of acceleration and the accelerometers are surface micro-machined silicon devices that use differential capacitance to sense acceleration.[10] The INS package on FIDO has a rate sensor range of 50 degrees per second and a sensitivity of approximately 25 degrees per second per volt. The range for the accelerometers is 2 g's with a sensitivity of 2 g's per volt. The interface to the unit is either through a RS232 serial link or via a direct analog output from the INS unit. Currently, the rate information is collected by the rover CPU at 50 Hz and numerically integrated at 50Hz to provide heading information.

4. EXPERIMENTAL RESULTS

The experimental results for determining the performance of each of the estimators were generated by running the FIDO rover in JPL's MarsYard. The MarsYard is an outdoor sand pit which contains a large number of rocks that are distributed throughout the pit according to typical rock distribution patterns found on Mars. The soil is

Movement number	Movement type	Movement number	Movement type
1	40 cm drive forward	12	40 cm drive forward
2	40 cm drive forward	13	30 degree turn-in-place
3	-30 degree turn-in-place	14	40 cm drive forward
4	40 cm drive forward	15	-20 degree turn-in-place
5	45 degree turn-in-place	16	40 cm drive forward
6	40 cm drive forward	17	40 cm drive forward
7	40 cm drive forward	18	40 cm drive forward
8	-45 degree turn-in-place	19	-45 degree turn-in-place
9	40 cm drive forward	20	40 cm drive forward
10	40 cm drive forward	21	40 cm drive forward
11	40 cm drive forward		

Table 1. Rover movement list.

generally soft and wheel slippage in this soil is usually encountered. For the tests described in this paper, the sun sensor is utilized as the primary heading sensor measurement. The INS package is used for attitude information for transforming the sun sensor information to the rover reference frame, however, as of now, the sensor information from the rate gyroscopes are not included in determining another measure of the rover's heading. In order to utilize the INS unit in the state estimation, the calculation/calibration of the rate sensor drift on the rover will be required while the rover is motionless. With the rate sensor drift accounted for in the determination of heading during motion, the INS will then be incorporated into the state estimation framework as outlined in this paper.

The rover carries a 266 MHz, Pentium-class CPU which runs the VxWorks 5.3 real-time operating system. All software for the FIDO rover is written in ANSI-C and is structured according to a three-layer architecture with the layers known as the driver layer, the device layer, and the application layer. All hardware dependancies are handled in the driver layer. The middle device layer provides the means for abstracting the higher level software in the application layer from the hardware dependencies. The device layer is responsible for all motion control functions, vision processing, instrument interfaces, forward and inverse kinematics for the rover and rover-mounted robot arms, etc. The application layer contains all rover sequences, instrument sequences, hazard detection and avoidance software, etc.

Ground truth information was collected using a differential GPS unit mounted on the rover in communication with a base station. Differential corrections are passed to the rover GPS unit via a wireless ethernet radio and the resulting accuracy of the position of the rover relative to the base station is $\pm$ 2 centimeters. The rover was commanded to move through various drive and turn-in-place maneuvers that covered a total of 6 meters of traverse. After each move, the rover automatically propagates and updates the rover's state estimate according to either the EKF estimation framework or the CI estimation framework discussed in the previous section. The list of rover movements are given in Table 1.

The results from the run that utilized the EKF as the state estimator are shown in Figure 4. For this run, the mean position error is 15.89 cm with a standard deviation of 10.43 cm over the 6 meter traverse. The results from the run that utilized the CI formulation as the state estimator are shown in Figure 4. The mean position error for this run is 15.44 cm with a standard deviation of 10.55 cm over the 6 meter traverse. For both of these runs, the assumed process noise covariance is chosen to be $\mathbf{Q} = \text{diag}[Q_{XX},\ Q_{YY},\ Q_{\phi\phi}] = [1\ \text{cm}^2,\ 1\ \text{cm}^2,\ 5\ \text{deg}^2]$, the measurement noise covariance is chosen to be $\mathbf{R} = 5\ \text{deg}^2$, and the initial estimation error covariance matrix is chosen to be $\mathbf{P}(0) = \text{diag}[P_{XX}(0),\ P_{YY}(0),\ P_{\phi\phi}(0)] = [10\ \text{cm}^2,\ 10\ \text{cm}^2,\ 10\ \text{deg}^2]$.

As seen in Figures 4 and 4, the results from the two runs are very similar. In part, this is due to the short nature of the rover traverse. It is expected that the Covariance Intersection results will, over time, be superior to the extended Kalman filter results since there will be strong correlation in time between the acquired measurements. This is due to the fact that there will be systematic biases and offsets that are not modeled in the calculation of the rover's heading by either the sun sensor or the INS package. Most likely, these biases will arise through the transformation of the sensor information from the sensor frame to the rover frame using attitude information which will have calibration errors that are not accounted for in the transformation. As such, this constant error source will produce

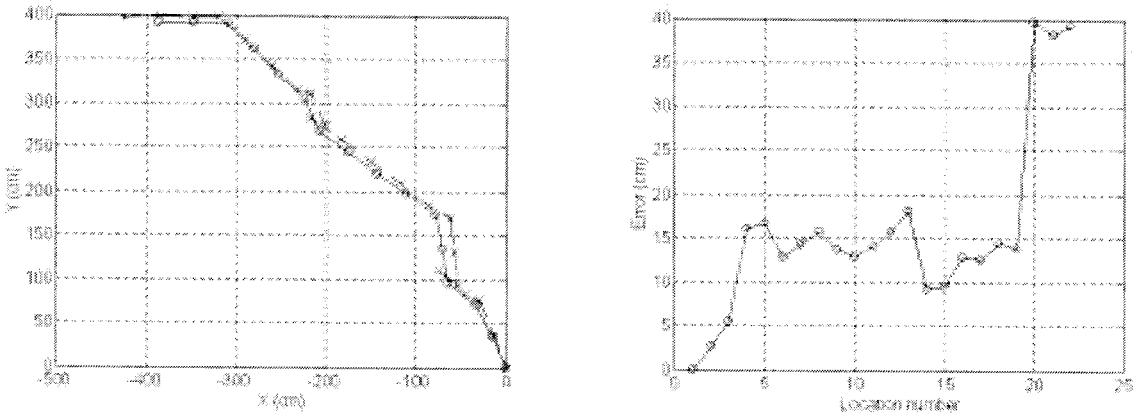

(a) Rover traverse

(b) Estimation error

Figure 4. EKF rover localization results.

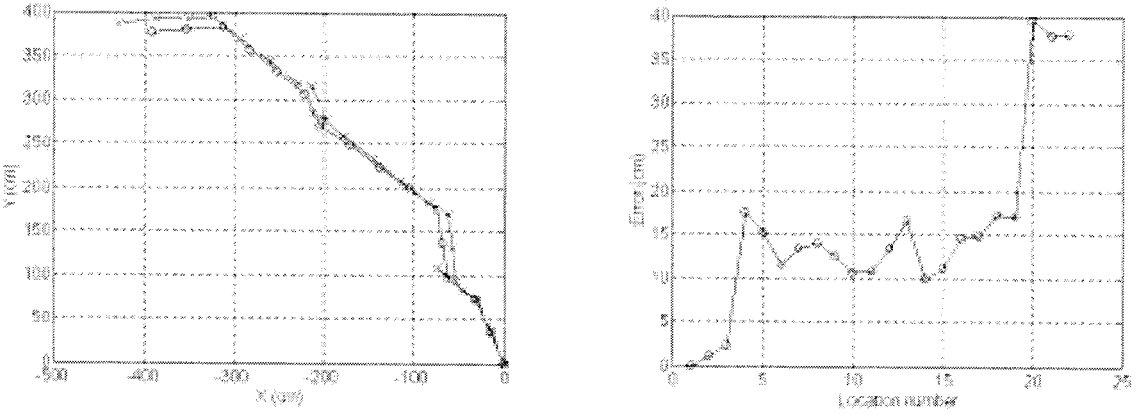

(a) Rover traverse

(b) Estimation error

Figure 5. CI rover localization results

time-correlated measurement readings that will effect the performance of the EKF state estimator which assumes the independance of measurement data. Since the CI-based estimator does not require uncorrelated measurement sources, it is expected that this filter will provide superior performance over long-duration rover traverses.

5. CONCLUSIONS

This paper has outlined the state estimation framework for generating fused rover localization information based on numerous sensor sources including wheel odometry, a sun sensor, and an inertial navigation sensor unit. The state estimation framework includes the use of two filter types, the extended Kalman filter and the Covariance Intersection approach. Experimental results are presented for rover traverses in JPL's MarsYard that indicate similar performance from both estimators. Future work will involve long-distance rover traverses in a natural terrain setting (arroyo wash) near the JPL campus. In these runs it is expected that the CI estimator will produce superior estimates when compared to the EKF-based approach due to the time correlation of the sensor measurements. Future work will also include the integration of the inertial navigation sensors in the state estimation framework to provide an additional measure of the rover's heading and visual map registration techniques for the measurement of the rover's traverse distance.

ACKNOWLEDGMENTS

The research described in this paper was carried out by the Jet Propulsion Laboratory, California Institute of Technology, under a contract with the National Aeronautics and Space Administration. The authors would like to thank Dr. Jeff Uhlmann, Unversity of Missouri, Columbia, and Dr. Simon Julier, Naval Research Laboratory, for their assistance with the Covariance Intersection approach and the base software used to produce the CI mean and covariance updates.

REFERENCES

1. E. T. Baumgartner, "In-Situ exploration of Mars using rover systems," to appear in *Proceedings of the AIAA Space 2000 Conference*, AIAA Paper 2000-5062, Long Beach, CA, September 2000.
2. P. S. Schenker, E. T. Baumgartner, R. A. Lindemann, H. Aghazarian, A. J. Ganino, G. S. Hickey, D. Q. Zhu, L. H. Matthies, B. H. Hoffman, and T. L. Huntsberger, "New planetary rovers for long-range mars science and sample return," Proceedings of SPIE, **3522**, pp. 2-15, Boston, MA, October 1998.
3. E. T. Baumgartner and S. B. Skarr, "An autonomous vision-based mobile robot," *IEEE Transactions on Automatic Control*, **39**(3), pp. 493-502, March 1994.
4. J.-D. Yoder, E. T. Baumgartner, and S. B. Skaar, "Initial results in the development of a guidance system for a power wheelchair," *IEEE Transactions on Rehabilitation Engineering*, **4**(3), pp. 143-151, September 1996.
5. J. Uhlmann, S. Julier, and M. Csorba, "Nondivergent simultaneous map building and localization using covariance intersection," *Proceedings of SPIE*, **3087**, pp. 2-11, June 1997.
6. B. H. Hoffman, E. T. Baumgartner, T. A. Huntsberger, and P. S. Schenker, "Improved State Estimation in Challenging Terrain," *Autonomous Robots*, **6**(2), pp. 113-130, April 1999.
7. C. F. Olson, "Probabilistic self-localization for mobile robots," *IEEE Transactions on Robotics and Automation*, **16**(1), pp. 55-66, February 2000.
8. L. Matthies, *Dynamic stereo vision*, Ph. D. Thesis, Canegie Mellon University, 1987.
9. Y. Xiong and K. Turkowski, "Creating image-based VR using self-calibrating fisheye lens," *Proceedings of IEEE Conference on Computer Vision and Pattern Recognition*, pp. 237-243, June 1997.
10. Crossbow Technology, Inc., *DMU User's Manual*, 1999.